*Paper based on L. R. Mills's Ph. D. thesis, Louisiana State University, 1970 (unpublished).

[1]H. Fröhlich, Advan. Phys. 3, 325 (1954).
[2]R. P. Feynman, Phys. Rev. 97, 660 (1955).
[3]J. Devreese and R. Evrard, Phys. Letters 23, 196 (1966).
[4]T. D. Schultz, Phys. Rev. 116, 526 (1959).

PHYSICAL REVIEW B VOLUME 2, NUMBER 8 15 OCTOBER 1970

Brillouin-Zone–Fermi-Surface Interactions in Pure and Lead-Doped Indium†

R. C. Carriker* and C. A. Reynolds
Physics Department and Institute of Materials Science, University of Connecticut, Storrs, Connecticut
(Received 17 February 1970)

Electrical resistivity anisotropies ($a \equiv \rho_\perp/\rho_\parallel$, direction referred to the c axis) of pure indium containing 0–9-at.% lead have been measured at 4.2, 77, and 273 °K. For pure indium it was found that $a(77) = 0.988 \pm 0.003$, while $a(273) = 1.037 \pm 0.003$; thus the direction of maximum resistivity changes from the c to the a direction as the temperature goes from 77 to 273 °K. This behavior is interpreted in terms of the resistivity anisotropy model of Klemens, Van Baarle, and Gorter, which is also used to qualitatively explain the observed anisotropies of the indium-lead alloys studied. Anomalies in the resistivity anisotropy were observed at 3.5- and 7.0 at. % lead, which were traced to anomalous behavior in the resistivity perpendicular to the c axis. The behavior at 7.0-at.% lead is interpreted as the Fermi surface popping through the (200) zone boundary. The temperature-dependent resistivity anisotropies of indium-lead alloys at 77 and 273 °K were determined, and at 273 °K, the direction of maximum temperature-dependent resistivity was found to change from the a to the c direction between 6- and 7-at. % lead. This behavior is attributed to an increasing perturbation of the indium lattice periodic potential by the lead ions at the relatively high temperature of 273 °K, and it is interpreted in terms of a breakdown in the δ-function potential approximation in the model of Klemens *et al.*

INTRODUCTION

Investigations in recent years on idium doped with lead have produced several interesting results in the 0–10-at. % region. These investigations have been concerned with superconducting transition temperature, [1,2] thermoelectric power, [3] electronic specific-heat coefficient, [2] and lattice spacings [4,5] of this system. If these various properties are plotted as a function of lead concentration, each will exhibit some interesting or "anomalous" behavior in the regions of 3.5- and 7.0-at. % lead, with the exception of the superconducting transition temperature which exhibits unusual behavior only near 7.0-at. % lead. These investigations gave impetus to the work reported here.

In the present investigation, nearly 100 cylindrical single-crystal specimens were prepared from pure indium and indium doped with 3–9 at. % lead. Approximately 80 of these specimens were considered to be of sample quality and had measurements made on them. Master alloys of 3.00-, 3.25-, 3.50-, 3.75-, 4.00-, 6.00-, 7.00-, 8.00-, and 9.00-at. % lead were prepared. A set of randomly oriented single-crystal samples was grown from each master alloy in addition to a set grown from pure indium.

The electrical resistivities along the cylindrical sample axis were measured at 4.2, 77, and 273 °K. In addition, the angle θ of the cystallographic c axis with respect to the cylindrical sample axis was determined for each sample. Since indium is tetragonal, the resistivity in a direction making an angle θ with the c axis can be written

$$\rho(\theta) = \rho_\perp + (\rho_\parallel - \rho_\perp)\cos^2\theta, \tag{1}$$

where $\rho_\parallel$ and $\rho_\perp$ are the resistivities parallel and perpendicular to the c axis. It is evident from Eq. (1) that a straight line drawn through the data for crystals of various orientations, plotted as ρ_{obs} versus $\cos^2\theta$, will yield $\rho_\parallel$ and $\rho_\perp$, and thus the resistivity anisotropy a, where $a \equiv \rho_\perp/\rho_\parallel$.

Although some work has been done on measuring the resistivities of pure indium [6–8] and indium doped with lead, [9–11] all of the previous work with the exception of that by Barisoni *et al.* [6] was done on polycrystalline samples and thus gives no direct measure of any anisotropies. We say "direct measure" because theoretical estimates of the anisotropy of the total resistivity can be made from polycrystalline data. For pure indium, Olsen [12] reported a value of 1.05 for the anisotropy at 273 °K. However, Olsen's value appears to have been a theoretical estimate based on polycrystalline data taken

from a table in the review paper by Gerritsen.[13] Barisoni *et al.* studied the anisotropy of the total resistivity of pure indium from 80 to 350 °K. They obtained a value of 1.034 for the anisotropy at 273 °K. Some caution must be used in accepting this value, since it is based on data from only two cylindrical single crystals, one oriented nearly parallel and one oriented nearly perpendicular to the c axis. No resistivity anisotropy information is available in the literature for indium doped with lead.

Extensive use will be made of the model of Klemens, Van Baarle, and Gorter[14] in interpreting our experimental results. Therefore, the principal features of the model, which is a modification of a model originally used by Harrison[15] for aluminum, will be briefly reviewed here. In order to calculate a resistivity anisotropy, one must first calculate the conductivities or resistivities in the directions of interest from an integral over the Fermi surface of the form

$$\sigma(\theta, \phi) = \frac{e^2}{4\pi^3 \hbar} \int \bar{v}_F \tau(\vec{k}) \cos^2 \psi \, dS_F, \qquad (2)$$

where σ is the conductivity in an arbitrary direction (θ, ϕ), e is the electronic charge, $\bar{v}_F$ is the average velocity at the Fermi surface, ψ is the angle between the direction (θ, ϕ) and the surface normal, and $\tau(\vec{k})$ is the anisotropic relaxation time. The heart of the model to be used is a scheme for weighing the effectiveness of the various portions of the Fermi surface in evaluating the integral in Eq. (2).

Klemens *et al.* begin by considering the Fermi surface to be a sphere in the extended zone scheme of momentum space. This sphere is divided into segments by those Brillouin-zone boundaries of nonvanishing structure factor which intersect it. In considering only those planes of nonvanishing structure factor, it is implicitly assumed that the electrons are nearly free and that the potential is constant everywhere except in the immediate vicinity of a lattice site, where it is approximately a δ-function potential. In the δ-function potential approximation, the appropriate structure factors appear as multiplicative factors in the Fourier components of the perturbating potential, and the relative effectiveness of the different zone boundaries in altering the electronic states is determined via the structure factors.[15] When the structure factor for a zone boundary is zero, there is no energy discontinuity across the boundary and electrons will not be scattered there. However, if the structure factor is nonzero, the electrons can be scattered (reflected) at the energy discontinuity, with the component of the electron's momentum along the normal to the reflection plane being reversed. These reflections can contribute to the resistive process by scattering electrons through large angles away from the current direction.

With the free-electron Fermi sphere broken into segments of various sizes by the zone boundaries with nonvanishing structure factor, the larger segments will be more effective in contributing to the conductivity, since electron states on these segments will have longer mean free paths. Also, the close proximity of zone boundaries in a small segment will cause small-angle scattering events which would normally be ineffective in contributing to the resistivity to become effective. This arises because an electron can reach a zone boundary via small angle scattering, where it can then suffer a large-angle Bragg scattering which will contribute to the resistivity. With this picture in mind, the regions of the Fermi sphere which are relatively finely divided by nonvanishing structure factor zone boundaries are ignored in taking the integral over the surface in Eq. (2). Effectively, the relaxation time is taken as a constant over the larger unbroken portions of the Fermi surface and zero over the smaller portions which are everywhere near a zone boundary. This is a good approximation only in the residual resistance regime or at high temperatures, since electrons experience large-angle scattering in both cases. In the case of intermediate temperatures when the ideal resistivity is dominant; i.e., for the case when $\rho_i(T) \gg \rho_0$, small-angle scattering prevails and the relaxation time increases rapidly as the distance from a zone boundary is increased. This causes the relative contribution to the conductivity of the larger unbroken segments of the Fermi surface to be even greater than in the large-angle scattering regimes.[14] It should be pointed out that care must be exercised in selecting the effective zone boundaries when the integration is carried out, since those zone boundaries with inverse lattice vectors normal to the direction in which the conductivity is being computed do not contribute to the resistive process.

Harrison[16] has shown that for polyvalent nontransition metals: (a) The electrons are nearly free; (b) the Fermi surface is nearly spherical; and (c) the effective potential or pseudopotential can be treated as a perturbation. In addition, Rayne,[17] Brandt and Rayne,[18] and Mina and Khaikin[19] have shown experimentally that the Fermi surface of indium is only slightly deformed from the free-electron surface. Therefore, we expect the resistivity anisotropy treatment of Klemens *et al.* to be particularly useful in the case of indium.

EXPERIMENTAL

Master alloys were prepared by carefully weighing out the proper proportions of 99.9999% pure indium[20] and lead[20] and melting them together under

a vacuum in a rocking furnace. A piece of master alloy was then remelted, baked out, and poured into a vertical precision bore Pyrex sample mold (~ 15 cm long with an inner diameter of 2.0000 ± 0.005 mm[21]) while under vacuum in a 300 °C sample-growing oven. The molten metal in its mold was then lowered out of the 300 °C sample-growing oven at a rate of 0.5 mm/min. The single-crystal specimen produced in this manner was then retrieved from the precision bore mold by etching away the glass with 48% hydrofluoric acid. This acid was also found to give the best sample surface etch prior to an orientation determination with an optical goniometer. The crystal orientation techniques used were those described by Gueths *et al.*[22] Once the crystal had been oriented, a 7-cm sample was cut from the crystal and annealed under vacuum at 110 °C for approximately 160 h.

The sample resistance determination technique of Burckbuchler and Reynolds[23] was used in the present investigation, with the sample resistance at 4.2, 77, and 273 °K being measured by the four-terminal potentiometric technique. The resistivities were considered to be accurate to within 0.7%, limited by geometrical uncertainties, most notably the diameter of the crystals.

RESULTS AND DISCUSSION

Resistivity Anisotropy of Pure Indium

The resistivity anisotropy of pure indium was determined at 77 and 273 °K, but not at 4.2 °K, because of the very high purity of the pure specimens.

Figures 1(a) and 1(b) show the resistivity anisotropy of pure indium at 77 and 273 °K, respectively. Figure 1(b) also includes data from samples measured prior to the present investigation.[24] Based on the data shown in the two figures, $a(77) = 0.988 \pm 0.003$ and $a(273) = 1.037 \pm 0.003$ for pure indium.

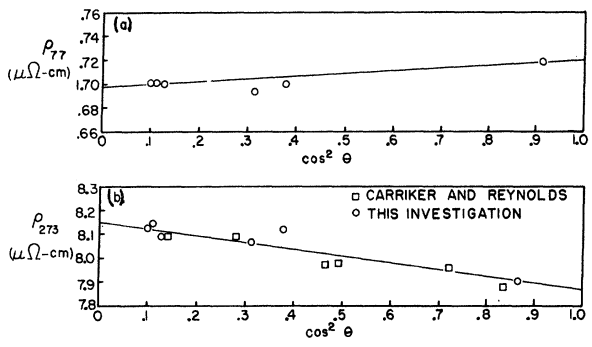

FIG. 1. (a) Graph used for the determination of the resistivity anisotropy of pure indium at 77 °K. (b) Graph used for the determination of the resistivity anisotropy of pure indium at 273 °K. ■: previous investigation in this laboratory (Ref. 24), ○: present investigation.

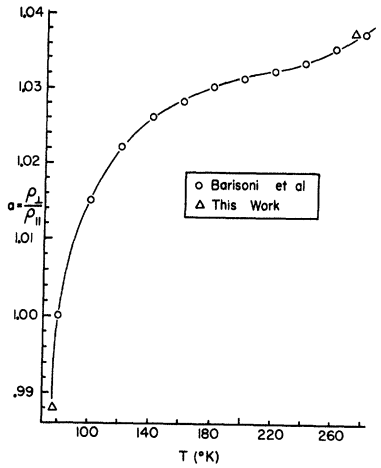

FIG. 2. Resistivity anisotropy of pure indium as a function of temperature from 77 to 280 °K. The figure indicates that the anisotropy goes below unity at ~ 80 °K. ○: Barisoni *et al.* (Ref. 6), △ : present work.

The very surprising aspect of these results is that the anisotropy of pure indium goes from below unity to above unity as the temperature is increased from 77 to 273 °K. That is, the resistivity along the c axis is greatest at 77 °K, but at 273 °K the direction of maximum resistivity has changed to the a direction. In examining Fig. 1(a), one might criticize the reliance on a single sample near $\cos^2\theta = 1.0$ to obtain the $a(77)$ value. There are two reasons why we feel we can rely on this sample. First, it fits on the 273 °K anisotropy plot [Fig. 1(b)] very well, indicating that the orientation is correct. Second, $a(77)$ from our data fits well on a plot of the resistivity anisotropy of pure indium as a function of temperature, shown in Fig. 2. The data for temperatures from 80 to 280 °K are those of Barisoni *et al*,[6] which were based on only two single-crystal samples of known orientation. Barisoni and his co-workers presented their data as $\rho_\parallel$ and $\rho_\perp$ versus temperature, and were apparently unaware of the trend for the anisotropy to go below unity near 80 °K. Since the differences between $\rho_\parallel$ and $\rho_\perp$ are small compared to their magnitudes, and since the difference decreases as the temperature approaches 80 °K, $\rho_\parallel$, and $\rho_\perp$ appear to converge to a common resistivity at 80 °K when both are plotted on an absolute scale as a function of temperature. However, plotting the data as we have done in Fig. 2, indicates that the anisotropy ($\rho_\perp/\rho_\parallel$) smoothly extrapolates to below unity in the vicinity of 80 °K.

Our value of $a(273)$ also fits very well on the anisotropy-versus-temperature curve shown in Fig. 2. Although Barisoni *et al.* did not report

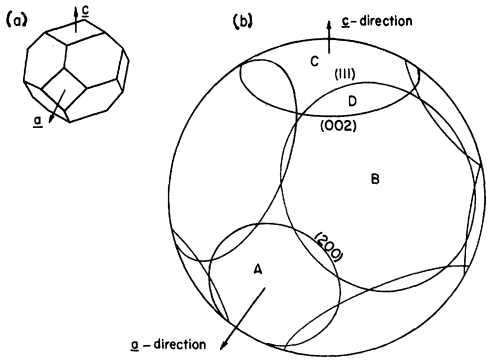

FIG. 3. (a) Nonvanishing structure factor zone surface for indium. (b) The intersections of the nonvanishing structure factor zone surface with the free-electron Fermi surface of indium.

values for $\rho_{\parallel}(273)$ and $\rho_{\perp}(273)$, they did report $a(273) = 1.034$, which they apparently obtained by interpolation. Their value is in good agreement with the 1.037 ± 0.003 found in this investigation.

In order to understand why the direction of maximum resistivity changes from the c and the a direction as the temperature goes from 77 to 273 °K, let us now invoke the resistivity anisotropy model of Klemens *et al.* Using the conventional picture of indium as a face-centered tetragonal lattice with atoms at (000), $(\frac{1}{2}\ \frac{1}{2}\ 0)$, $(\frac{1}{2}\ 0\ \frac{1}{2})$, and $(0\ \frac{1}{2}\ \frac{1}{2})$, there are only three sets of zone boundaries with nonzero structure factor that intersect the free-electron Fermi surface, namely, (111), (200), and (002).[25] Figure 3(a) shows the nonvanishing structure factor zone surface (Jones zone) formed by these zones. Figure 3(b) shows how intersections with this surface segment the free-electron Fermi surface.

To find the contribution of a segment of Fermi surface to the conductivity in a given direction, we use an integral of the form

$$I_s = \frac{3}{(2\pi)} \int \cos^2 \psi \, dS, \tag{3}$$

where ψ is the angle between the direction for which the conductivity is being computed and the surface normal. The factor $3/2\pi$ normalizes the integral to unity relative to a free-electron gas, where one hemisphere of the Fermi surface contributes to the conductivity. That is, the integral is normalized relative to a free-electron gas with the same mean free path. We will generally find it more convenient to calculate I_s for those areas which do not contribute to the conductivity and then subtract from unity to obtain the conductivity. To avoid any confusion, the reader is reminded that zone boundaries with their inverse lattice vectors normal to the direction in which the conductivity is being computed should not be included.

The (200) zone boundaries are very nearly tangential to the Fermi surface. It is highly probable that the Fermi surface extending beyond these zones is much smaller than shown in Fig. 3(b). It is even quite possible that there is no overlap of the zone boundary by the Fermi surface. Whatever the precise situation, this area (A) will be considered as not contributing to the conductivity in the a direction. The regions marked D in Fig. 3(b) are small and are everywhere close to a zone boundary. Therefore, these regions will not be included in finding the conductivity.

Let us now examine the resistivity anisotropy at 273 °K. We first consider the conductivity in the a direction. The cap formed in the a direction by the (200) zone boundary (segment A) subtends an angle of approximately 22° from the a direction. However, in order to take into account the small segments at 90° intervals around the periphery of this cap, we take the zone boundary angle to be on the order of 24°. Integrating over this effective cap yields $I_s = 0.24$. In considering the conductivity in the c direction, we consider only the D segments as not contributing to the conductivity. These segments subtend approximately 12.5° at their widest point, centered at about 25° from the c direction. We approximate the four D segments by a circular ring 10° wide, centered at 25° from the c direction. Integration over this ring yields $I_s = 0.18$. The anisotropy is then

$$a(273) = \frac{\rho_{\perp}}{\rho_{\parallel}} = \frac{\sigma_{\parallel}}{\sigma_{\perp}} = \frac{1.00 - 0.18}{1.00 - 0.24} = 1.08, \tag{4}$$

which agrees well with the experimental value of 1.037, especially in view of the approximations made in estimating Fermi-surface areas.

We now proceed to the calculation of the anisotropy at 77 °K, $a(77)$. At this temperature, small-angle scattering would be expected to reduce the relative contribution to the conductivity of the smaller unbroken areas of the Fermi surface. Looking at Fig. 3(b), it can be seen that segment C is relatively small compared to the B segments. Thus we will consider C in addition to the A and D segments to be ineffective in contributing to the conductivity at 77 °K relative to the contribution of the B segments. In reality $l_B > l_C > l_A$ (l is the electronic mean free path), so that the true anisotropy should be less extreme than that we are calculating. The cap of Fermi surface in the c direction formed by the intersection with the (002) zone boundary subtends an angle of approximately 31.5° from the c direction (this cap includes segments C and D). Integrating over this cap gives $I_s = 0.38$. Thus the relative conductivity in the c direction is 1.00–0.38. For the conductivity in the a direction, the

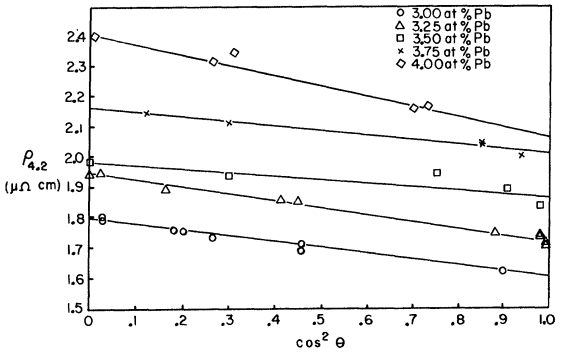

FIG. 4. Plots used for the determination of the residual resistivity ($\rho_{4.2}$) anisotropies of indium doped with 3.00-, 3.25-, 3.50-, 3.75-, and 4.00-at. % lead.

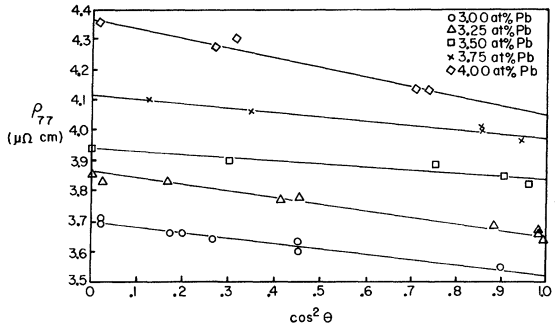

FIG. 6. Plots used for the determination of the anisotropies of the total resistivity at 77 °K for indium doped with 3.00-, 3.25-, 3.75-, and 4.00-at. % lead.

segment A is treated as it was for the 273 °K case, since in both instances A does not contribute to the conductivity. Recalling that $I_s = 0.24$ for A, we obtain a resistivity anisotropy of

$$a(77) = (1.00 - 0.38)/(1.00 - 0.24) = 0.82 . \quad (5)$$

This is somewhat smaller than the experimentally determined value of 0.988, although the fact that a figure less than unity was obtained is probably more significant than the quantitative difference. That is, the correct sense of the anisotropy was found (we shall always refer to the quality of the anisotropy of being either above or below unity as the "sense" of the anisotropy). The difference between the experimental and calculated anisotropies is probably due to an overestimation in the effectiveness of small-angle scattering in reducing the conductivity contribution of the cap at the c axis. This cap or segment is large enough so that its central area may be too far removed from the zone boundaries to be greatly affected by small-angle scattering. As the central unaffected area is increased, the calculated anisotropy approaches the experimental value.

Total Resistivity Anisotropy of Indium-Lead Alloys

The residual resistivity anisotropies (4.2 °K) of the 3–8-at. % lead alloys are shown in Figs. 4 and 5. The electrical resistivity anisotropy at 4.2 °K of the 9-at. % lead alloy could not be determined, since this alloy is a type-II superconductor at this temperature. The anisotropies of the total resistivity at 77 °K for the 3–9-at. % lead alloys are shown in Figs. 6 and 7, while those at 273 °K are shown in Figs. 8 and 9. Numerical values for the anisotropies shown in these figures are given in Table I.

We shall begin the discussion of the alloy resistivity anisotropies by confining our attention to the sense of the anisotropies shown in Figs. 4–9, delaying for the moment the discussion of the variation in anisotropy with doping.

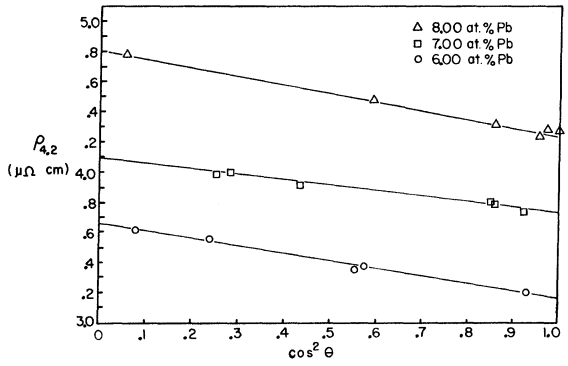

FIG. 5. Plots used for the determination of the residual resistivity ($\rho_{4.2}$) anisotropies of indium doped with 6.00-, 7.00-, and 8.00-at. % lead. The 9.00-at. % samples are not included since they were superconducting (type II) at 4.2 °K.

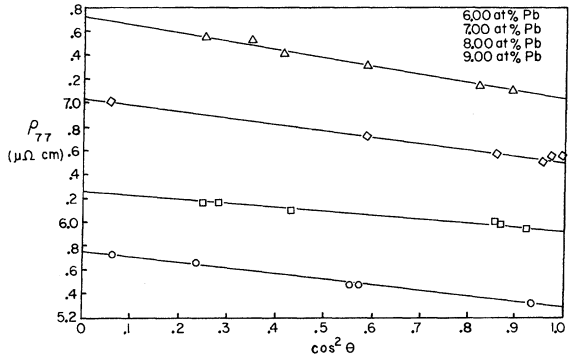

FIG. 7. Plots used for the determination of the anisotropies of the total resistivity at 77 °K for indium doped with 6.00-, 7.00-, 8.00-, and 9.00-at. % lead.

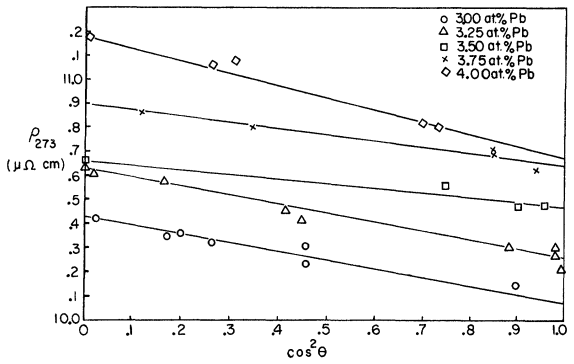

FIG. 8. Plots used for the determination of the anisotropies of the total resistivity at 273 °K for indium doped with 3.00-, 3.25-, 3.50-, 3.75-, and 4.00-at. % lead.

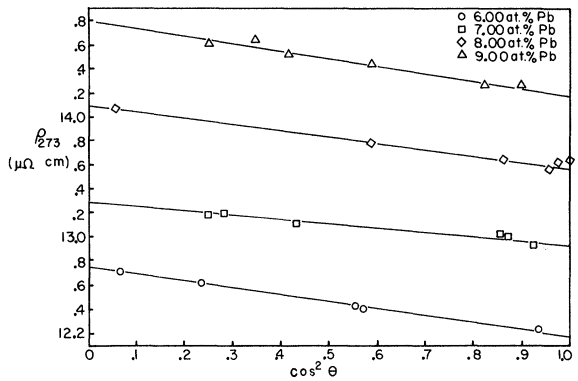

FIG. 9. Plots used for the determination of the anisotropies of the total resistivity at 273 °K for indium doped with 6.00-, 7.00-, 8.00-, and 9.00-at % lead.

The anisotropy model of Klemens *et al.* is equivalent for the residual resistivity and high-temperature regimes, since large-angle scattering dominates the resistive process in both. Because of this, the resistivity anisotropy would be expected to have the same qualitative appearance (sense) at 4.2 °K as it does at 273 °K, although perhaps not the same quantitative behavior (magnitude). Table I indicates that this is the case for the indium-lead alloys.

The lattice spacing data for indium doped with lead indicates that there is a decrease in the distances of the zone boundaries from the origin, which is typically on the order of 0.5% in going from pure indium to indium doped with 8.0-at. % lead. Over the same range of doping, k_F for the free-electron Fermi sphere increases by approximately 0.3%. This increase in k_F was calculated with the valence Z replaced by an effective valence $Z_{\text{eff}} = 3(1-x)+4(x)$. The factors 3 and 4 refer to the valences of indium and lead, respectively, and x is the lead concentration in at. %. The change in volume of the unit cell with doping was also taken into account in the calculation of the change in k_F.

TABLE I. Anisotropy of the total resistivity at 4.2, 77, and 273 °K for indium + 0–9-at. % lead alloys.

at. %	$a(4.2)$	$a(77)$	$a(273)$
0.00	···	0.988	1.037
3.00	1.123	1.047	1.035
3.25	1.134	1.055	1.036
3.50	1.060	1.023	1.018
3.75	1.079	1.035	1.024
4.00	1.162	1.074	1.047
6.00	1.158	1.088	1.046
7.00	1.096	1.055	1.028
8.00	1.130	1.082	1.039
9.00	···	1.098	1.044

Thus, it is apparent that there is only a slight change in the position of the Fermi surface relative to the zone boundaries. This relative shift in position does not significantly affect our picture of the segmented Fermi surface as shown in Fig. 3(b). In addition, the estimates involved in obtaining a resistivity anisotropy from the model being used would not allow a calculation of the change in anisotropy for such a small adjustment in relative position.

From the above arguments, we conclude that the residual resistivity anisotropy and the total resistivity anisotropy at 273 °K for our indium-lead alloys should be approximately that already calculated for pure indium at 273 °K, namely, $a \simeq 1.08$. Table I indicates that this gives the proper sense of the anisotropies (4.2 and 273 °K), with a magnitude which is approximately correct for both. Actually 1.08 lies approximately between $a(273)$ and $a(4.2)$, with $a(273)$ always being less than $a(4, 2)$ for a given alloy. This feature $[a(273) < a(4.2)]$, along with the structure in the residual resistivity anisotropy as a function of doping still must be dealt with. However, this discussion must be delayed until further groundwork has been laid.

For pure indium, the anisotropy had a different sense at 77 °K than at 273 °K. Table I indicates that this is not the case for the indium with 3–9-at. % lead alloys. In order to explain this, let us focus on the 3.0-at. % lead alloy, although the general line of reasoning will be applicable for the other alloys as well. We will assume that the total resistivity is given by Matthiessen's rule,

$$\rho_T = \rho_0 + \rho_i(T), \tag{6}$$

where ρ_0 is the residual resistivity and ρ_T and $\rho_i(T)$ are the total and ideal resistivities, respectively, at a temperature T. This assumption will suffice

for our qualitative arguments, since even in the worst case (8.0 at. %), the deviation from Matthiessen's rule at 77 °K is only on the order of 8% of ρ_{77}. The residual resistivity of the 3.0-at. % alloys is on the order of 1.75 $\mu\Omega$cm, while the ideal resistivity at 77 °K is on the order of 1.71 $\mu\Omega$cm. Here the resistivity of pure indium is being used as the ideal resistivity, since $\rho_0 \simeq 0$ for our pure specimens. In addition to being larger (alloys with an impurity content > 3.0 at. % have even larger ρ_0's), the residual resistivity of the 3.0-at. % alloys has a much stronger anisotropy than the ideal resistivity at 77 °K (1.123 versus 0.988, respectively). Because of the relative magnitudes of these two resistivity contributions and their anisotropies, it appears that increased large-angle scattering brought on by increased impurity content is dominant over the effect of small-angle scattering that might have been expected at 77 °K. This leads to the resistivity anisotropy of the alloys at 77 °K having the same sense as the residual resistivity. We will show later that the temperature-dependent resistivity anisotropy of the alloys at 77 °K is the same as the ideal resistivity anisotropy at 77 °K. This supports our view that the residual resistivity anisotropy is still dominant at 77 °K for the alloys.

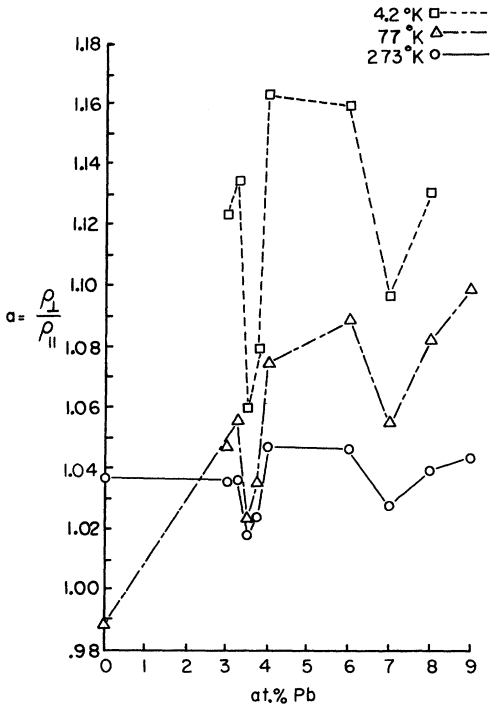

FIG. 10. Plot of the anisotropies of the total resistivities at 4.2, 77, and 273 °K as a function lead impurity content in indium for 0–9-at. % lead. Figure clearly indicates structure at 3.5- and 7.0-at% lead.

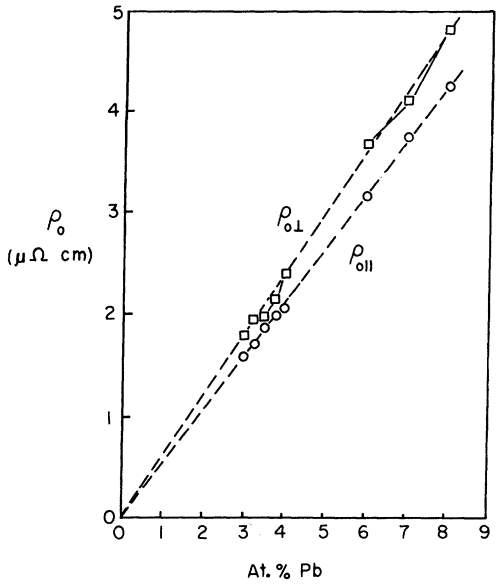

FIG. 11. Plot of the residual resistivities parallel and perpendicular to the *c* axis for indium-lead alloys as a function of lead content for 3-8-at. % lead. Figure indicates that the structure in the anisotropy (Fig. 10) is due to unusual behavior in the resistivity for the *a* direction.

Fermi-Surface–Brillouin-Zone Interactions

We now turn our attention to the variation in total resistivity anisotropy as a function of lead content. The effects of doping on the anisotropies of the total resistivity at 4.2, 77, and 273 °K are shown in Fig. 10. In this figure, the anisotropies at the three given temperatures are plotted as a function of at. % lead. From the figure, it is readily apparent that something occurs near 3.5 and 7.0 at. %, producing structure in the anisotropy versus concentration plots. It should be pointed out that the structure in the 77 and 273 °K plots is merely a reflection of the structure in the residual resistivity anisotropy, so that this structure can be attributed to something occurring in the residual resistance regime. The impurity concentrations for this observed structure correlate well with the concentrations giving structure in other properties of indium doped with lead previously mentioned.

The structure in the anisotropy, shown in Fig. 10, indicates an interaction of some type between the Brillouin zone and the Fermi surface. However, it does not indicate on which part of the Fermi surface this interaction occurs. In Fig. 11 the alloy residual resistivities parallel and perpendicular ($\rho_{0\parallel}$ and $\rho_{0\perp}$, respectively) are plotted as a function of at. % lead. This figure clearly indicates that the observed structure in the residual resistivity anisotropy is due to anomalous behavior in $\rho_{0\perp}$ as a

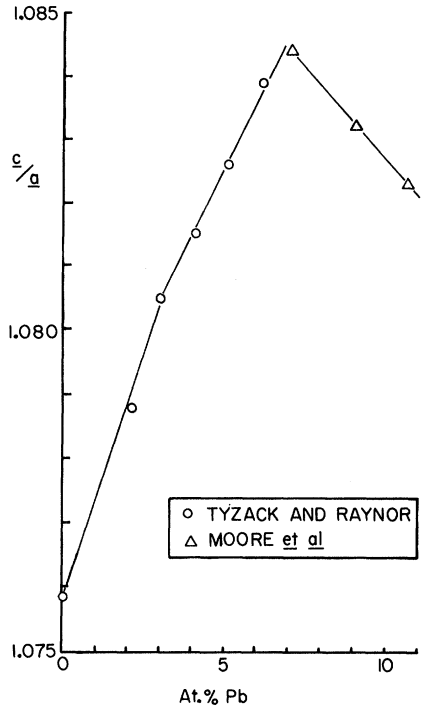

FIG. 12. Plot of the ratio of the lattice spacings c/a for indium as a function of lead content from 0- to 10-at.% lead. Note that there is a slight change in slope at ~3.0-at.% lead. The ○ are the data of Tyzack and Raynor (Ref. 4) and the △ are the data of Moore *et al* (Ref. 5).

function of lead content. Therefore, interactions in or near the a direction in reciprocal space should be sought to explain this behavior.

With reference to the data displayed in Fig. 11, the residual resistivity parallel to the c axis increases at a rate of 0.53-$\mu\Omega$cm/at.% lead for 0–8-at.% lead. Excluding the regions of structure, the resistivity in the a direction for the same concentration range increases at an average rate of 0.60-$\mu\Omega$cm/at.% lead. The values available in the literature are in this range, although they are for polycrystalline specimens. Noto *et al.*[10] and Gygax *et al.*[11] have reported values of 0.60-$\mu\Omega$ cm/at.% lead and 0.55-$\mu\Omega$cm/at.% lead, respectively.

To explain Figs. 10 and 11, we will make use of the lattice spacing data of Tyzack and Raynor[4] as amended by Moore *et al.*[5], and the treatment of Goodenough[26] for changes in c/a due to Brillouin-zone–Fermi-surface interactions with increasing electron-atom ratio z. Figure 12 shows c/a versus at.% for indium doped with lead. There is a slight change in slope near 3.5 at.% and a change in the sign of the slope near 7.0 at.%.

In the discussion that follows, the interaction of the (111) zone boundaries with the Fermi surface will not be mentioned. As can be seen in Fig. 3(b), the overlap of these zone boundaries by the Fermi surface is complete or nearly so and they would not be expected to be effective in producing changes in c/a. In addition, any interactions of the Fermi surface with the (111) zone boundaries should not be too effective in producing changes in c/a due to their nearly symmetrical position with respect to the c and a directions.

The $\rho_{0\perp}$ anomalies found in the present investigation and the c/a behavior of the indium-lead alloys suggest a possible sequence of events as lead is added to indium up to approximately 9.0 at.%. We cannot be too specific in the interpretation of the data, since changes in c/a and $\rho_{0\perp}$ only give indirect evidence as to precisely what is occurring.

We postulate that for pure indium, the Fermi surface overlaps the (002) zone boundaries, but only intersects the (200) zone boundaries without overlapping them. This is not only supported by the evidence to be discussed, but is also supported by the fact that this view was used to successfully calculate $a(273)$ for pure indium. As lead is added to the indium, the Fermi surface moves out and the overlap of the (002) boundaries becomes greater. The increased partial pressure of the overlapping electrons would tend to push the (002) zone boundaries toward the center of the zone. This effect would tend to increase c/a. At the same time, the (200) boundaries are pushed away from the origin by the expanding Fermi surface. This would also lead to an increase in c/a. This picture is suggested by the fact that c/a increases as lead is added up to approximately 3.5 at.%.

At approximately 3.5 at.%, the Fermi surface undergoes some sort of adjustment in the a direction. Although we do not know the detailed nature of this adjustment, it is such that more Fermi surface becomes available to contribute to the conductivity in the a direction, as evidenced by a slight decrease in $\rho_{0\perp}$ from linearity (see Fig. 11). This adjustment is also evidenced by a change in slope of the c/a versus at.% lead in the vicinity of 3.5 at.%. As lead (and thus z) is increased beyond 3.5 at.%, this slope continues to be positive as before, but with a reduced magnitude. A plot of the 0–6-at.% lead data of Tyzack and Raynor for the lattice spacings as a function of alloying indicates that the change in slope of c/a at ~3.5-at.% lead is due to a change in the rate that a increases with lead content. This supports our resistivity evidence which points to a Fermi-surface–Brillouin-zone interaction in the a direction near 3.5-at.% lead.

At approximately 7.0 at.%, some overlap of the (200) zone boundaries probably begins. This is strongly suggested by a change to decreasing c/a as the doping increases beyond 7.0 at.%. Once

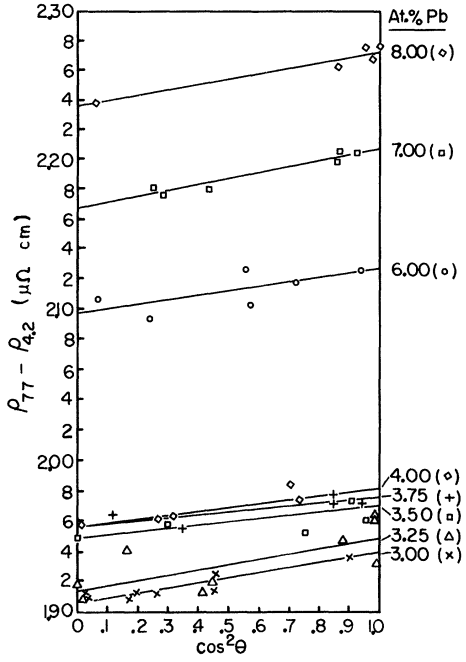

FIG. 13. Plots used for the determination of the temperature-dependent resistivity ($\rho_{77} - \rho_{4.2}$) anisotropies at 77 °K for indium doped with 3.00-, 3.25-, 3.50-, 3.75-, 4.00-, 6.00-, 7.00-, and 8.00-at. % lead. Note jump in $\rho_{77} - \rho_{4.2}$ at 3.25–3.50-at. % lead.

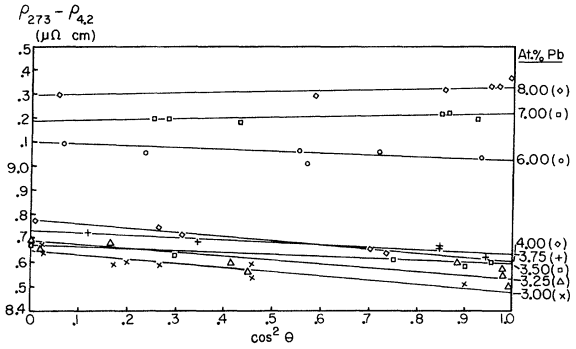

FIG. 14. Plots used for the determination of the temperature-dependent resistivity ($\rho_{273} - \rho_{4.2}$) anisotropies at 273 °K for indium doped with 3.00-, 3.25-, 3.50-, 3.75-, 4.00-, 6.00-, 7.00-, and 8.00-at. % lead. The general trend is a gradual decrease in the anisotropy ($\rho_\perp/\rho_\parallel$) until it goes below unity at 6–7-at. % lead.

overlap is initiated, the partial pressure of the overlapping electrons on the (200) zone boundaries would cause them to move toward the center of the zone. This would cause c/a to decrease with increasing z. The possibility of overlap of the (200) zone boundaries is further supported by the slight increase in the conductivity near 7.0 at. %, since the overlapping segment would produce a small contribution to the conductivity which was nonexistent before overlap occurred. Examination of Fig. 14 of Moore *et al.* indicates that the change in c/a at 7-at. % lead is due to an increase in the slope of a versus at. % lead. This supports our resistivity evidence that the Brillouin-zone–Fermi-surface interaction at ~ 7 at. % lead is in the a direction.

Temperature-Dependent Resistivity Anisotropy

The temperature-dependent resistivities of the 3–8-at. % lead alloy samples at 77 and 273 °K were obtained by subtracting the residual resistivity ($\rho_{4.2}$) from the total resistivities at 77 and 273 °K (ρ_{77} and ρ_{273}). The temperature-dependent resistivity anisotropies were then obtained by plotting $\rho_{77} - \rho_{4.2}$ and $\rho_{273} - \rho_{4.2}$ versus $\cos^2\theta$ for each alloy. The temperature-dependent resistivity anisotropies at 77 and 273 °K are shown in Fig. 13 and 14, respectively. A temperature-dependent resistivity anisotropy will be denoted by the subscript i, even though we realize that there is a contribution due to the deviation from Matthiessen's rule. Values of $a_i(77)$ and $a_i(273)$ for the alloys are tabulated in Table II.

The anisotropy at 77 °K, $a_i(77)$, is essentially constant as a function of doping, maintaining a value of 0.986 ± 0.004 from 3.0–8.0-at. % lead. Between 3.25- and 3.50-at. % lead there is a jump in the magnitude of the temperature-dependent resistivity at 77 °K (see Fig. 13), but the anisotropy remains more or less constant in spite of this anomalous behavior. In the neighborhood of 3.50–4.00-at. % lead, $a_i(273)$ fluctuates slightly, but the general trend appears to be a gradual reduction in $a_i(273)$ as the doping is increased to 6.0 at. %. In the vicinity of 7.0-at. % lead, the sense of $a_i(273)$ reverses and we find $a_i(273) < 1.0$ for 7.0- and 8.0-at. % lead.

We will first give attention to $a_i(77)$. Since $a(77)$ for pure indium was found to be 0.988, while $a_i(77)$ for the 3–8-at. % lead alloys was found to be 0.986

TABLE II. Anisotropy of the temperature-dependent resistivity at 77 and 273 °K for indium +3–9-at. % lead alloys.

at. %	$a_i(77)$	$a_i(273)$
3.00	0.988	1.020
3.25	0.983	1.018
3.50	0.989	1.009
3.75	0.990	1.012
4.00	0.987	1.020
6.00	0.986	1.008
7.00	0.983	0.997
8.00	0.985	0.996
9.00	• • •	• • •

± 004, the anisotropy of the temperature-dependent resistivity at 77 °K does not change throughout the entire range from pure indium to indium doped with 8.0-at. % lead. We thus conclude that our model of the effective zones giving rise to the resistivity anisotropy of pure indium at 77 °K remains correct for $a_i(77)$ up to 8.0-at. % lead. Since the temperature-dependent resistivity increases, while its anisotropy remains constant as a function of increasing impurity content, we conclude that the mechanism giving rise to the deviation from Matthiessen's rule is isotropic or very nearly so at 77 °K. The reason for the jump in the temperature-dependent resistivity in the region of 3.25–3.50 at. % is not clear. It is difficult to imagine a mechanism which would cause this type of event without a corresponding change in the anisotropy.

We shall not attempt to explain the small variations in $a_i(273)$ in going from 3.0- to 6.0-at. % lead. The approximate nature of the model being used to discuss resistivity anisotropy will not permit subtle changes such as these to be analyzed. We only note here that $a_i(273)$ for the 3–6-at. % lead alloys has the same sense as $a(273)$ for pure indium (the ideal resistivity anisotropy at 273 °K), which is the sense one would expect from our model, since nothing new has been introduced in our Fermi-surface–zone-boundary picture. The model must be improved in order to explain the general trend in $a_i(273)$; viz., the reduction in the anisotropy from that of the pure case as the lead content is increased until the sense of $a_i(273)$ finally reverses around 7.0-at. % lead.

Consideration of Zero Structure Factor Zone Boundaries

To this point we have proceeded by considering only the zone boundaries of nonvanishing structure factor. We have had reasonable success in explaining the generally observed anisotropies. However, within the framework of this model using nonvanishing structure factor zone boundaries, we have been unable to explain the change in the sense of $a_i(273)$ in the vicinity of 6–7-at. % lead. We will now consider those zero structure factor zone boundaries which intersect the Fermi surface.

We suspect that the zero structure factor zone boundaries should be included for the dirtier alloys, especially at elevated temperatures. The model of resistivity anisotropy that we have been using implicitly assumes that the potential of an ion at a lattice site can be well represented by a δ function. We suspect that two factors contribute to the breakdown of this assumption. The first factor is the increasing lead content, since the potential of a lead ion in the indium lattice does not approximate a δ-function potential as well as the indium ion does in its own lattice. When a lead ion is introduced, it will produce a strain field in the indium lattice. In addition, there will be a redistribution of charge to shield the valence difference of the lead ion. This will be accomplished by a long-range electronic charge density oscillation which falls off as the third power with distance from the impurity site.[27,28] The strain field and the charge density oscillation would be particularly effective in causing a breakdown of the δ-function potential approximation, since they are long range by comparison. The second factor leading to a breakdown of the δ-function potential assumption is the thermal motion of the ions at their lattice sites at elevated temperatures. When the δ-function potential approximation breaks down, the perturbing potentials at the zone boundaries no longer have the appropriate structure factors as simple multiplicative constants which measure the effectiveness of the zone boundaries. Thus as the δ-function potential approximation is relaxed, the effectiveness of zone boundaries which originally had zero structure factor would increase relative to the effectiveness of the zone boundaries with nonvanishing structure factor.

Figure 15 shows the intersections of the zero structure factor zone boundaries with the Fermi surface. Ignoring for the moment the segments formed by the intersections with the (102) zone boundaries, there is little to differentiate between the a and c directions. That is, the segmenting of the Fermi surface by the zero structure factor zone boundaries looks approximately the same whether

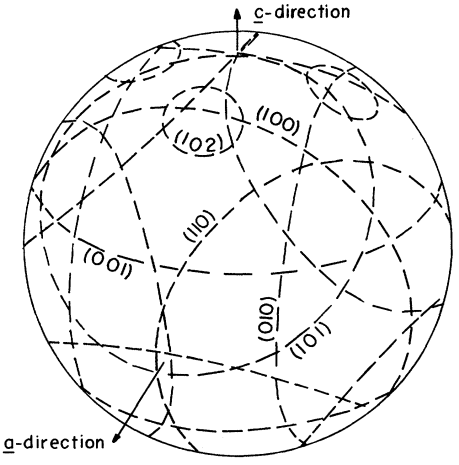

FIG. 15. Intersections of zone boundaries having zero structure factor with the free-electron Fermi surface for the case of indium. Careful examination indicates that the figure looks approximately the same for the c and a directions with the exception of the (102) zone boundary intersections.

viewed along the a direction or along the c direction. However, when these zone boundaries are included with those of nonvanishing structure factor, they gain significance in the c direction. In the calculation of the resistivity anisotropy at 273 °K the central region of the cap in the c direction was considered to contribute to the conductivity. The segmenting of this region by the zero structure factor zones could thus reduce the conductivity in the c direction. In addition, the (102) zone boundaries intersect the Fermi surface near the c direction with no similar intersections near the a direction, since the (201) zone boundaries lie just outside the Fermi surface. The cap in the a direction was taken to be ineffective in contributing to the conductivity. Therefore, the division of this cap by the zero structure factor zone boundaries would have no effect on the conductivity in the a direction.

From the last two paragraphs we may conclude that the relative importance of the zero structure factor zone boundaries probably only becomes significant for the more heavily doped alloys at elevated temperatures. In addition, the inclusion of these zone boundaries significantly affects the conductivity only in the c direction by segmenting the region near the c direction which had previously contributed to the conductivity. Since we expect the zero structure factor zone boundaries to become effective only at elevated temperatures with increasing impurity concentration, the general trend in $a_i(273)$ to decrease with doping until it finally goes below unity at 6–7 at. % is explained with the inclusion of these zone boundaries. Also, since $a = \sigma_{\parallel}/\sigma_{\perp}$, the relative reduction in the conductivity in the c direction at elevated temperatures explains the feature noted earlier that $a(273)$ is less than $a(4.2)$ for the alloys.

SUMMARY

The resistivity anisotropies of pure indium at 77 and 273 °K were measured and the direction of maximum resistivity was found to change from the c to the a direction as the temperature is increased from 77 to 273 °K. An explanation of this effect was found using the resistivity anisotropy model of Klemens, Van Baarle, and Gorter, which was used to interpret the sense of the resistivity anisotropies observed in this investigation. In addition, anomalous behavior in the resistivity anisotropy of indium-lead alloys as a function of lead content in the regions of 3.5- and 7.0-at. % lead was observed, and was traced to structure in the resistivity normal to the c axis. Both the results of this investigation and the lattice spacing data available in the literature are found to support the view that the structure observed at 7.0-at. % lead is due to the Fermi surface popping through the (200) zone boundary at this concentration. Finally, the temperature-dependent resistivity anisotropy was examined as a function of lead content at 77 and 273 °K. The direction of maximum temperature-dependent resistivity at 273 °K was found to change from the a to the c direction between 6- and 7-at. % lead, and this behavior was interpreted in terms of a breakdown of the δ-function potential approximation in the model of Klemens *et al.*

ACKNOWLEDGMENTS

The authors wish to express their appreciation to Professor P. G. Klemens for many valuable discussions during the course of this investigation. The authors also wish to thank Dr. F. V. Burckbuchler for many informative discussions, H. Taylor for technical assistance, and D. Strom for technical assistance and preparation of the illustrations.

---

†Work supported in part by the U. S. Air Force Office of Scientific Research (Grant No. AF-AFOSR-474-67) and the Office of Naval Research [Contract No. NONR 2967 (00)].

*Present address: United Aircraft Research Laboratories, East Hartford, Conn.

[1]M. F. Merriam, Phys. Rev. Letters 11, 321 (1963); Rev. Mod. Phys. 36, 152 (1964).

[2]S. Gygax, J. L. Olsen, and R. H. Kropschot, in *Proceedings of the Ninth International Conference on Low Temperature Physics, Columbus, Ohio*, 1964, edited by J. G. Daunt (Plenum, New York, 1965).

[3]W. J. Tomasch and J. R. Reitz, Phys. Rev. 111, 757 (1958).

[4]C. Tyzack and G. Raynor, Trans. Faraday Soc. 50, 675 (1954).

[5]A. Moore, J. Graham, G. K. Williamson, and G. V. Raynor, Acta Met. 3, 579 (1955).

[6]M. Barisoni, R. K. Williams, and D. L. McElroy, Proceedings of the Seventh Conference on Thermal Conductivity, Natl. Bur. Stand., Gaithersburg, Md. (unpublished).

[7]E. Grüneisen, Ergebn. Exakt. Naturw. 21, 50 (1945).

[8]W. Meissner and B. Voigt, Ann. Physik 7, 761 (1930); 7, 892 (1930).

[9]B. N. Aleksandrov, Fiz. Metal. Metalloved. 14, 434 (1962).

[10]K. Noto, Y. Muto, and T. Fukuroi, J. Phys. Soc. Japan 21, 2122 (1966).

[11]S. Gygax, J. L. Olsen, and R. H. Kropschot, Phys. Letters 8, 228 (1964).

[12]J. L. Olsen, *Electron Transport in Metals* (Interscience, New York, 1962).

[13]A. N. Gerritsen, *Handbuch der Physik*, edited by S. Flügge (Springer, Berlin, 1956), Vol. 19.

[14]P. G. Klemens, C. Van Baarle, and F. W. Gorter, Physica 30, 1470 (1964).

[15]W. A. Harrison, Phys. Rev. 118, 1190 (1960).

[16]W. A. Harrison, Phys. Rev. 129, 2503 (1963).
[17]J. A. Rayne, Phys. Rev. 129, 652 (1962).
[18]G. B. Brandt and J. A. Rayne, Phys. Rev. 132, 1512 (1963); Phys. Letters 12, 87 (1964).
[19]R. T. Mina and M. S. Khaikin, Zh. Eksperim. i Teor. Fiz. 51, 62 (1966) [Soviet Phys. JETP 24, 42 (1966)].
[20]Obtained from United Mineral and Chemical Corp., New York, N. Y.
[21]Obtained from Wilmad Glass Co., Buena, N. J.
[22]J. F. Gueths, F. V. Burckbuchler, and C. A. Reynolds, Rev. Sci. Instr. 40, 1344 (1969).
[23]F. V. Burckbuchler and C. A. Reynolds, Phys. Rev. 175, 550 (1968).
[24]R. C. Carriker and C. A. Reynolds, Bull. Am. Phys. Soc. 14, 98 (1969).
[25]Throughout this paper we will distinguish n_3 from n_1 and n_2, but not n_1 from n_2 in the set $(n_1\, n_2\, n_3)$, because of symmetry.
[26]J. B. Goodenough, Phys. Rev. 89, 282 (1953).
[27]J. Friedel, Phil. Mag. 43, 153 (1952); Advan. Phys. 3, 446 (1954).
[28]W. Kohn and S. H. Vosko, Phys. Rev. 119, 912 (1960).

PHYSICAL REVIEW B VOLUME 2, NUMBER 8 15 OCTOBER 1970

Tunneling Spectroscopy in Degenerate p-Type Silicon†

D. E. Cullen,* E. L. Wolf,‡ and W. Dale Compton§
Coordinated Science Laboratory and Department of Physics, University of Illinois, Urbana, Illinois 61801
(Received 24 February 1970)

Tunneling in boron-doped p-type silicon metal-semiconductor (MS) and metal-insulator-semiconductor (MIS) tunnel junctions has been studied at low temperatures by measuring the derivatives dI/dV and d^2I/dV^2 of the current-voltage characteristics as functions of applied bias voltage V. The boron impurity concentration of the silicon crystals varied from 6.5×10^{18} to $2.3\times10^{20}\,\mathrm{cm}^{-3}$. Junctions were prepared by evaporating metal contacts onto vacuum- or air-cleaved silicon surfaces. The general features of the tunneling conductance were found to be in qualitative agreement with existing theories of tunneling in semiconductors. Structure in the derivative data resulting from the interaction of tunneling electrons with silicon zone-center optical phonons and boron local-mode phonons has been observed. The optical-phonon line shapes in the most heavily doped MIS units are shown to compare well with the theoretical line shapes in which modifications in the bulk semiconductor states arising from electron–optical-phonon interactions in the semiconductor electrode have been included. The origin of the optical-phonon and local-mode-phonon structure in samples of lower doping is not fully understood.

I. INTRODUCTION

Tunneling in a wide variety of semiconductor systems has been studied over the past several years. A critical review of much of this work has recently been given by Duke.[1] Of particular importance to the present work are the studies that have been made of processes involving inelastic tunneling, namely, electronic tunneling with the assistance of phonons.[2,3] Such processes are exemplified by a steplike increase in conductance at a bias corresponding to the energy of the participating phonon. These effects are symmetric about zero bias. In a measurement d^2I/dV^2 (i.e., dG/dV), such effects are seen as antisymmetric peaks.

Wolf[4] first presented data on the tunneling into p-type silicon that clearly showed symmetric peaks in d^2I/dV^2 at the energies of the zone-center optical phonon. He suggested that such effects arise from a modification in the electronic dispersion relations resulting from electron-phonon interactions. Davis and Duke[5] have shown quantitatively how such modifications can affect the structure in the tunneling conductance. They have made a detailed calculation of the shapes of the lines in d^2I/dV^2 versus V that result from these many-body interactions and have compared these calculated line shapes with experimental measurements.

This paper is primarily concerned with the electron–optical-phonon and electron–local-mode-phonon interactions in degenerate p-type silicon as revealed in electron tunneling spectra. Preliminary experimental results have already been presented[4,6] as have related theoretical studies.[7,8] We present here more extensive experimental results, with particular attention to the systematic changes that occur as a function of the concentration of the boron dopant. It is shown that the observed line shapes agree with the Davis and Duke formalism only at high doping levels. It is suggested that at the lower doping levels the properties of the barrier begin to dominate and that the